

**Canonical-basis time-dependent Hartree-Fock-Bogoliubov theory and linear-response calculations**Shuichiro Ebata,<sup>1,2</sup> Takashi Nakatsukasa,<sup>1,3</sup> Tsunenori Inakura,<sup>1</sup> Kenichi Yoshida,<sup>1</sup> Yukio Hashimoto,<sup>2,3</sup> and Kazuhiro Yabana<sup>1,2,3</sup><sup>1</sup>*RIKEN Nishina Center, Wako-shi 351-0198, Japan*<sup>2</sup>*Graduate School of Pure and Applied Sciences, University of Tsukuba, Tsukuba 305-8571, Japan*<sup>3</sup>*Center for Computational Sciences, University of Tsukuba, Tsukuba 305-8571, Japan*

(Received 6 July 2010; published 9 September 2010)

We present simple equations for a canonical-basis (Cb) formulation of the time-dependent Hartree-Fock-Bogoliubov (TDHFB) theory. The equations are obtained from the TDHFB theory with an approximation that the pair potential is assumed to be diagonal in the Cb. The Cb formulation significantly reduces the computational cost. We apply the method to linear-response calculations for even-even light nuclei and demonstrate its capability and accuracy by comparing our results with recent calculations of the quasiparticle random-phase approximation with Skyrme functionals. We show systematic studies of  $E1$  strength distributions for Ne and Mg isotopes. The evolution of the low-lying pygmy strength seems to be determined by the interplay of several factors, which include the neutron excess, the separation energy, the neutron-shell effects, the deformation, and the pairing.

DOI: [10.1103/PhysRevC.82.034306](https://doi.org/10.1103/PhysRevC.82.034306)

PACS number(s): 21.60.Jz, 25.20.Dc, 24.30.Cz, 27.30.+t

**I. INTRODUCTION**

The time-dependent Hartree-Fock (TDHF) theory was extensively applied to studies of nuclear collective phenomena as a microscopic approach to nuclear dynamics [1]. Recently, it has been revisited with modern energy density functionals, and a more accurate description of nuclear properties has been achieved [2–7]. The TDHF theory uses only occupied orbitals, the number of which is equal to the number of particles ( $N$ ), to describe a variety of nuclear dynamics, such as heavy-ion scattering, fusion/fission phenomena, and linear-response functions. However, it neglects the residual interactions in particle-particle (p-p) and hole-hole (h-h) channels, which becomes problematic especially for open-shell heavy nuclei. An alternative approach, which includes the pairing correlations, is the time-dependent Hartree-Fock-Bogoliubov (TDHFB) theory [8]. The TDHFB equation is formulated in a similar manner to the TDHF; however, it uses the quasiparticle orbitals instead of the occupied orbitals. Since the number of the quasiparticle orbitals is, in principle, infinite, the accurate calculation of TDHFB is presently impractical. Only recently, have a few attempts of the TDHFB calculation been performed, but either with a small model space [9] or with a restriction to spherical symmetry [10].

A much simpler approach was proposed by Błocki and Flocard in Ref. [11]. They gave equations of motion for time-dependent canonical states  $|\phi_k(t)\rangle$  ( $k = 1, \dots, M$ ) and those for the time-dependent BCS factors  $[u_k(t), v_k(t)]$ . Since the number of the canonical basis (Cb) is larger than the particle number but not significantly different ( $M \sim N$ ), the necessary computational task is roughly the same as that of TDHF. Similar methods have been applied to studies of heavy-ion reactions with the use of simple functionals [12–14]. However, it has never been tested with realistic modern functionals so far, and we do not know how reliable this approximated scheme is. In addition, although the equations of motion were provided for a very schematic pairing functional in Ref. [11], its theoretical foundation seems rather obscure to us.

In this paper, we derive the equations of motion for general functionals and clarify the approximations/assumptions we need to make. We call those equations canonical-basis time-dependent Hartree-Fock-Bogoliubov (Cb-TDHFB) equations. We apply the method to the linear-response calculations by using the full Skyrme functionals. The results will be compared with recent calculations of the quasiparticle random-phase approximation (QRPA), then will demonstrate its feasibility and accuracy.

The paper is organized as follows. In Sec. II, we present the basic equations of the present method and their derivation. Especially, we would like to clarify what kind of assumption/approximation is necessary to justify the Cb-TDHFB equations. In Sec. III, we show properties of the Cb-TDHFB, which include the gauge invariance, the conservation laws, and the small-amplitude limit. In numerical calculations in this paper, we adopt a schematic choice for the pairing energy functional, similar to Ref. [11], which violates the gauge invariance. In Sec. IV, we show that the effect of the violation of the gauge invariance can be minimized by a special choice of the gauge condition. In Sec. V, details of our numerical installation are given. Then, in Sec. VI, we present numerical results for the real-time calculations of the linear response and compare them with recent QRPA/random-phase approximation (RPA) calculations. Finally, the conclusion is given in Sec. VII.

**II. DERIVATION OF BASIC EQUATIONS**

In this section, we derive the basic equations of the Cb-TDHFB method. By using the time-dependent variational principle, similar equations were derived by Błocki and Flocard [11]. However, what kind of approximation was introduced and how it was different from the full TDHFB were not clear. Here, we present a sufficient condition to reduce the TDHFB equations to those in a simple canonical form.

We start from the density-matrix equation of the TDHFB and find equations for the Cb states and their occupation- and

pair-probability factors. To clarify our heuristic strategy, let us start from a simpler case without the pairing correlation.

### A. TDHF equation

The TDHF equation in the density-matrix formalism is written as [15]

$$i \frac{\partial}{\partial t} \rho(t) = [h(t), \rho(t)], \quad (1)$$

where  $\rho(t)$  and  $h(t)$  are the one-body density operator and the single-particle (Hartree-Fock [HF]) Hamiltonian, respectively. We now express the one-body density by using the time-dependent canonical single-particle basis  $\{|\phi_k(t)\rangle\}$ , which is assumed to be orthonormal [ $\langle\phi_k(t)|\phi_l(t)\rangle = \delta_{kl}$ ],

$$\rho(t) = \sum_{k=1}^N |\phi_k(t)\rangle \langle\phi_k(t)|, \quad (2)$$

where  $N$  is the total particle number. By substituting this into Eq. (1), we have

$$\begin{aligned} & \sum_{k=1}^N \{i \dot{|\phi_k(t)\rangle} \langle\phi_k(t)| + i |\phi_k(t)\rangle \langle\dot{\phi}_k(t)|\} \\ &= \sum_{k=1}^N \{h(t) |\phi_k(t)\rangle \langle\phi_k(t)| - |\phi_k(t)\rangle \langle\phi_k(t)| h(t)\}. \end{aligned} \quad (3)$$

The inner product with  $|\phi_k(t)\rangle$  leads to

$$\hat{P} \left[ i \frac{\partial}{\partial t} - h(t) \right] |\phi_k(t)\rangle = 0, \quad k = 1, \dots, N, \quad (4)$$

with  $\hat{P} = 1 - \sum_{k=1}^N |\phi_k(t)\rangle \langle\phi_k(t)|$ . Here, we used the conservation of the orthonormal property for the canonical states  $d/dt \langle\phi_k(t)|\phi_l(t)\rangle = 0$ . This leads to the most general Cb-TDHF equations,

$$\begin{aligned} i \frac{\partial}{\partial t} |\phi_k(t)\rangle &= h(t) |\phi_k(t)\rangle - \sum_{l=1}^N |\phi_l(t)\rangle \eta_{lk}(t), \\ &k = 1, \dots, N, \end{aligned} \quad (5)$$

where the matrix  $\eta_{lk}(t)$  is arbitrary but should be Hermitian to conserve the orthonormal property. It is easy to see that the time evolution of the density does not depend on the choice of  $\eta_{lk}$ . This is related to the gauge invariance with respect to the unitary transformations among  $|\phi_k(t)\rangle$  ( $k = 1, \dots, N$ ). The most common choice is  $\eta_{lk} = 0$ , which leads to the TDHF equation shown in most textbooks.

### B. Cb-TDHFB equations

We now derive Cb-TDHFB equations that start from the generalized density-matrix formalism. The TDHFB equation can be written in terms of the generalized density matrix [8] as

$$i \frac{\partial}{\partial t} R = [\mathcal{H}, R], \quad (6)$$

where

$$R \equiv \begin{pmatrix} \rho & \kappa \\ -\kappa^* & 1 - \rho^* \end{pmatrix}, \quad \mathcal{H} \equiv \begin{pmatrix} h & \Delta \\ -\Delta^* & -h^* \end{pmatrix}. \quad (7)$$

This is equivalent to the following equations for the one-body density matrix  $\rho(t)$  and the pairing-tensor matrix  $\kappa(t)$ :

$$\begin{aligned} i \frac{\partial}{\partial t} \rho(t) &= [h(t), \rho(t)] + \kappa(t) \Delta^*(t) - \Delta(t) \kappa^*(t), \quad (8) \\ i \frac{\partial}{\partial t} \kappa(t) &= h(t) \kappa(t) + \kappa(t) h^*(t) \\ &\quad + \Delta(t) [1 - \rho^*(t)] - \rho(t) \Delta(t). \end{aligned} \quad (9)$$

At each instant of time, we may diagonalize the density operator  $\hat{\rho}$  in the orthonormal Cb  $\{|\phi_k(t)\rangle, |\phi_{\bar{k}}(t)\rangle\}$  with the occupation probabilities  $\rho_k$ . For the canonical states, we use the alphabetic indexes such as  $k$  for half of the total space indicated by  $k > 0$ . For each state with  $k > 0$ , there exists a paired state  $\bar{k} < 0$ , which is orthogonal to all the states with  $k > 0$ . The set of states  $\{|\phi_k\rangle, |\phi_{\bar{k}}\rangle\}$  generates the whole single-particle space.<sup>1</sup> We use the Greek letters  $\mu, \nu, \dots$  for indexes of an adopted representation (complete set) for the single-particle states. The creation operator of particles at the state  $|\phi_k(t)\rangle$  is expressed as  $\hat{c}_k^\dagger(t) = \sum_{\mu} \langle\mu|\phi_k(t)\rangle \hat{c}_{\mu}^\dagger$ , and the TDHFB state is expressed in the canonical (BCS) form as

$$|\Psi(t)\rangle = \prod_{k>0} \{u_k(t) + v_k(t) \hat{c}_k^\dagger(t) \hat{c}_{\bar{k}}^\dagger(t)\} |0\rangle. \quad (10)$$

For later purposes, it is convenient to introduce the following notations for two-particle states:

$$\langle\mu\nu|\phi_k(t)\phi_{\bar{k}}(t)\rangle \equiv \langle\mu|\phi_k(t)\rangle \langle\nu|\phi_{\bar{k}}(t)\rangle, \quad (11)$$

$$\langle\langle\mu\nu|\phi_k(t)\phi_{\bar{k}}(t)\rangle\rangle \equiv \langle\mu\nu|\phi_k(t)\phi_{\bar{k}}(t)\rangle - \langle\mu\nu|\phi_{\bar{k}}(t)\phi_k(t)\rangle, \quad (12)$$

and for the projection operator on a canonical pair of states  $(k, \bar{k})$ ,

$$\hat{\pi}_k(t) \equiv |\phi_k(t)\rangle \langle\phi_k(t)| + |\phi_{\bar{k}}(t)\rangle \langle\phi_{\bar{k}}(t)|. \quad (13)$$

Then, it is easy to show the following properties ( $k, l > 0$ ):

$$\sum_{\mu\nu} \langle\mu\nu|\phi_k(t)\phi_{\bar{k}}(t)\rangle \langle\phi_l(t)\phi_{\bar{l}}(t)|\mu\nu\rangle = \delta_{kl}, \quad (14)$$

$$\sum_{\mu\nu} \langle\langle\mu\nu|\phi_k(t)\phi_{\bar{k}}(t)\rangle\rangle \langle\langle\phi_l(t)\phi_{\bar{l}}(t)|\mu\nu\rangle\rangle = 2\delta_{kl}, \quad (15)$$

$$\sum_{\sigma} \langle\langle\mu\sigma|\phi_k(t)\phi_{\bar{k}}(t)\rangle\rangle \langle\langle\phi_l(t)\phi_{\bar{l}}(t)|\nu\sigma\rangle\rangle = \delta_{kl} \langle\mu|\hat{\pi}_k(t)|\nu\rangle, \quad (16)$$

$$\sum_{\sigma} \langle\langle\mu\sigma|\phi_k(t)\phi_{\bar{k}}(t)\rangle\rangle \langle\nu|\hat{\pi}_l(t)|\sigma\rangle = \delta_{kl} \langle\langle\mu\nu|\phi_k(t)\phi_{\bar{k}}(t)\rangle\rangle. \quad (17)$$

By using these notations, the density and the pairing-tensor matrices are given by

$$\rho_{\mu\nu}(t) = \sum_{k>0} \rho_k(t) \langle\mu|\hat{\pi}_k(t)|\nu\rangle, \quad (18)$$

$$\kappa_{\mu\nu}(t) = \sum_{k>0} \kappa_k(t) \langle\langle\mu\nu|\phi_k(t)\phi_{\bar{k}}(t)\rangle\rangle, \quad (19)$$

<sup>1</sup>In the case without pairing ( $\Delta = 0$ ), the canonical pair becomes arbitrary as far as they have the same occupation probabilities  $\rho_k$  that are either 1 or 0.

where  $\rho_k(t)$  and  $\kappa_k(t)$  are occupation and pair probabilities, respectively. In terms of the BCS factors of  $(u, v)$  [15], they are given as  $\rho_k(t) = |v_k(t)|^2$  and  $\kappa_k(t) = u_k^*(t)v_k(t)$ . It should be noted that the canonical pair of states  $|\phi_k(t)\rangle$  and  $|\phi_{\bar{k}}(t)\rangle$  are assumed to be orthonormal but not necessarily related with each other by the time reversal  $|\phi_{\bar{k}}\rangle \neq T|\phi_k\rangle$ .

Thanks to the orthonormal property, we can invert Eqs. (18) and (19) for  $\rho_k$  and  $\kappa_k$ ,

$$\begin{aligned}\rho_k(t) &= \sum_{\mu\nu} \langle \phi_k(t)|\mu\rangle \rho_{\mu\nu}(t) \langle \nu|\phi_k(t)\rangle \\ &= \sum_{\mu\nu} \langle \phi_{\bar{k}}(t)|\mu\rangle \rho_{\mu\nu}(t) \langle \nu|\phi_{\bar{k}}(t)\rangle,\end{aligned}\quad (20)$$

$$\begin{aligned}\kappa_k(t) &= \sum_{\mu\nu} \langle \phi_k(t)\phi_{\bar{k}}(t)|\mu\nu\rangle \kappa_{\mu\nu}(t) \\ &= \frac{1}{2} \sum_{\mu\nu} \langle\langle \phi_k(t)\phi_{\bar{k}}(t)|\mu\nu\rangle\rangle \kappa_{\mu\nu}(t).\end{aligned}\quad (21)$$

With the help of Eq. (18), the derivative of  $\rho_k(t)$  with respect to time  $t$  leads to

$$\begin{aligned}i \frac{d}{dt} \rho_k(t) &= \sum_{\mu\nu} \langle \phi_k(t)|\mu\rangle i \frac{d\rho_{\mu\nu}}{dt} \langle \nu|\phi_k(t)\rangle \\ &\quad + i \rho_k(t) \frac{d}{dt} \langle \phi_k(t)|\phi_k(t)\rangle \\ &= \sum_{\mu\nu} \langle \phi_k(t)|\mu\rangle i \frac{d\rho_{\mu\nu}}{dt} \langle \nu|\phi_k(t)\rangle \\ &= \sum_{\mu\nu} \{ \kappa_k(t) \Delta_{\mu\nu}^*(t) \langle \nu\mu|\phi_k(t)\phi_{\bar{k}}(t)\rangle \\ &\quad + \kappa_k^*(t) \Delta_{\mu\nu}(t) \langle \phi_k(t)\phi_{\bar{k}}(t)|\mu\nu\rangle \}.\end{aligned}\quad (22)$$

We used the assumption of norm conservation for the second equation, and used the TDHFB equation Eq. (8) in the last equation. Since the pair potential  $\Delta_{\mu\nu}(t)$  is antisymmetric, it is written in a simple form as

$$\begin{aligned}i \frac{d}{dt} \rho_k(t) &= \kappa_k(t) \Delta_k^*(t) - \kappa_k^*(t) \Delta_k(t), \\ \Delta_k(t) &\equiv - \sum_{\mu\nu} \Delta_{\mu\nu}(t) \langle \phi_k(t)\phi_{\bar{k}}(t)|\mu\nu\rangle \\ &= - \frac{1}{2} \sum_{\mu\nu} \Delta_{\mu\nu}(t) \langle\langle \phi_k(t)\phi_{\bar{k}}(t)|\mu\nu\rangle\rangle.\end{aligned}\quad (23)$$

In the case where the pair potential is computed from a two-body interaction  $v$  as  $\Delta_{\mu\nu}(t) = \sum_{\alpha\beta} v_{\mu\nu,\alpha\beta} \kappa_{\alpha\beta}(t)$ , the gap parameters  $\Delta_k(t)$  are identical to those of the BCS approximation [15]:

$$\Delta_k(t) = - \sum_{l>0} \kappa_l(t) (v_{k\bar{k},l\bar{l}} - v_{k\bar{k},l\bar{l}}) \equiv - \sum_{l>0} \kappa_l(t) \bar{v}_{k\bar{k},l\bar{l}}.\quad (25)$$

Here, it should be noted that the two-body matrix elements  $v_{k\bar{k},l\bar{l}}$  (and the antisymmetric  $\bar{v}_{k\bar{k},l\bar{l}}$ ) are time dependent because the canonical bases  $(k, \bar{k})$  and  $(l, \bar{l})$  are time dependent.

In the same way, we evaluate the time derivative of  $\kappa_k(t)$  as

$$\begin{aligned}i \frac{d}{dt} \kappa_k(t) &= \sum_{\mu\nu} \langle \phi_k(t)\phi_{\bar{k}}(t)|\mu\nu\rangle i \frac{d\kappa_{\mu\nu}}{dt} \\ &\quad + i \kappa_k(t) \left[ \left\langle \frac{d\phi_k}{dt} \middle| \phi_k(t) \right\rangle + \left\langle \frac{d\phi_{\bar{k}}}{dt} \middle| \phi_{\bar{k}}(t) \right\rangle \right].\end{aligned}\quad (26)$$

Then, by using the TDHFB equation Eq. (9), we obtain

$$i \frac{d}{dt} \kappa_k(t) = [\eta_k(t) + \eta_{\bar{k}}(t)] \kappa_k(t) + \Delta_k(t) [2\rho_k(t) - 1],\quad (27)$$

where  $\eta_k(t) \equiv \langle \phi_k(t)|h(t)|\phi_k(t)\rangle + i \langle \frac{\partial \phi_k}{\partial t} | \phi_k(t) \rangle$ .

The time-dependent equations for  $\rho_k(t)$  and  $\kappa_k(t)$  are now given in rather simple forms as Eqs. (23) and (27). So far, their derivation is solely based on the TDHFB equations, by utilizing the fact that  $\rho_{\mu\nu}(t)$  and  $\kappa_{\mu\nu}(t)$  can be expressed by the orthonormal canonical bases  $|\phi_k(t)\rangle$  and  $|\phi_{\bar{k}}(t)\rangle$  and their occupation and pair probabilities  $\rho_k(t)$  and  $\kappa_k(t)$ . However, in general, the time evolution of the Cb is not given by a simple equation. Therefore, we now introduce an assumption (approximation) that the pair potential is written as

$$\Delta_{\mu\nu}(t) = - \sum_{k>0} \Delta_k(t) \langle\langle \mu\nu|\phi_k(t)\phi_{\bar{k}}(t)\rangle\rangle.\quad (28)$$

This satisfies Eq. (24), but, in general, Eq. (24) cannot be inverted because the two-particle states  $|\phi_k\phi_{\bar{k}}\rangle$  do not span the whole space. In other words, we only take the pair potential of the diagonal parts in the Cb  $\Delta_{k\bar{l}} = -\Delta_k \delta_{kl}$  into account. In the stationary limit ( $|\phi_{\bar{k}}\rangle = T|\phi_k\rangle$ ), this is equivalent to the ordinary BCS approximation (see Sec. III C).

With the approximation of Eq. (28), it is easy to see that the TDHFB equations Eqs. (8) and (9) are consistent with the following equations:

$$\begin{aligned}i \frac{\partial}{\partial t} |\phi_k(t)\rangle &= [h(t) - \eta_k(t)] |\phi_k(t)\rangle, \\ i \frac{\partial}{\partial t} |\phi_{\bar{k}}(t)\rangle &= [h(t) - \eta_{\bar{k}}(t)] |\phi_{\bar{k}}(t)\rangle.\end{aligned}\quad (29)$$

To summarize, the Cb-TDHFB equations consist of Eqs. (23), (29), and (27). To derive these equations from the TDHFB equations, we have assumed the diagonal property of the pair potential Eq. (28).

### III. PROPERTIES OF THE Cb-TDHFB EQUATIONS

#### A. Gauge invariance

The  $\eta_k(t)$  and  $\eta_{\bar{k}}(t)$  in Eqs. (27) and (29) must be real to conserve the orthonormal property, however, they are arbitrary. This is related to the phase degrees of freedom of the canonical states. The Cb-TDHFB equations Eqs. (23), (27), and (29) are invariant with respect to the following gauge transformations with arbitrary real functions  $\theta_k(t)$  and  $\theta_{\bar{k}}(t)$ :

$$|\phi_k\rangle \rightarrow e^{i\theta_k(t)} |\phi_k\rangle \quad \text{and} \quad |\phi_{\bar{k}}\rangle \rightarrow e^{i\theta_{\bar{k}}(t)} |\phi_{\bar{k}}\rangle,\quad (30)$$

$$\kappa_k \rightarrow e^{-i[\theta_k(t)+\theta_{\bar{k}}(t)]} \kappa_k \quad \text{and} \quad \Delta_k \rightarrow e^{-i[\theta_k(t)+\theta_{\bar{k}}(t)]} \Delta_k\quad (31)$$

simultaneously with

$$\eta_k(t) \rightarrow \eta_k(t) + \frac{d\theta_k}{dt} \quad \text{and} \quad \eta_{\bar{k}}(t) \rightarrow \eta_{\bar{k}}(t) + \frac{d\theta_{\bar{k}}}{dt}.\quad (32)$$

The phase relations of Eq. (31) are obtained from Eqs. (21) and (24).

## B. Conservation laws

### 1. Orthonormality of canonical states

Apparently, Eq. (29) conserves the orthonormal property of canonical states, as far as  $\eta_k$  are real:

$$i \frac{\partial}{\partial t} \langle \phi_k(t) | \phi_l(t) \rangle = \langle \phi_k(t) | \{ [h(t) - \eta_l(t)] - [h^\dagger(t) - \eta_k(t)] \} | \phi_l(t) \rangle = 0. \quad (33)$$

Here, we assume  $\langle \phi_k(t) | \phi_l(t) \rangle = \delta_{kl}$  at time  $t$ .

### 2. Average particle number

The average particle number also conserves because

$$i \frac{d}{dt} N(t) = 2i \frac{d}{dt} \sum_{k>0} \rho_k(t) = 2 \sum_{k>0} [\kappa_k(t) \Delta_k^*(t) - \kappa_k^*(t) \Delta_k(t)] = 0, \quad (34)$$

where we used the expression of the pairing energy Eq. (60) for the last equation.

### 3. Average total energy

Time variation of the energy functional  $E[\rho, \kappa]$  can be divided into two:  $dE/dt = dE/dt|_\rho + dE/dt|_\kappa$ . The variation of energy associated with the normal-density fluctuation is

$$i \left. \frac{dE}{dt} \right|_\rho = i \sum_{\mu\nu} \frac{\partial E}{\partial \rho_{\mu\nu}} \frac{d\rho_{\mu\nu}}{dt} = i \sum_{k>0} \frac{d\rho_k}{dt} [\epsilon_k(t) + \epsilon_{\bar{k}}(t)], \quad (35)$$

where  $\epsilon_k(t) = \langle \phi_k(t) | h(t) | \phi_k(t) \rangle$ . This equation has an intuitive physical interpretation. The energy carried by a canonical state  $|\phi_k\rangle$  is  $\epsilon_k(t) \times \rho_k$ . If the occupation probability is fixed during the time evolution, the right-hand side of Eq. (35) vanishes. This corresponds to cases such as the TDHF and its extension with fixed BCS occupation probabilities. In the TDHFB, the energy variation in Eq. (35) transfers from/to the pairing energy. In fact, time variation caused by the pairing tensors produces fluctuation,

$$i \left. \frac{dE}{dt} \right|_\kappa = i \frac{1}{2} \sum_{\mu\nu} \left( \frac{\partial E}{\partial \kappa_{\mu\nu}} \frac{d\kappa_{\mu\nu}}{dt} + \frac{\partial E}{\partial \kappa_{\mu\nu}^*} \frac{d\kappa_{\mu\nu}^*}{dt} \right) = \sum_{k>0} (\kappa_k^* \Delta_k - \kappa_k \Delta_k^*) [\epsilon_k(t) + \epsilon_{\bar{k}}(t)], \quad (36)$$

where Eq. (28) is used. Because of Eq. (23), two contributions of Eqs. (35) and (36) always cancel, and the total energy is conserved. This is natural because the Cb-TDHFB equations satisfy the TDHFB equations Eqs. (8) and (9) for which the conservation of the total energy in TDHFB is well known [8].

## C. Stationary solution

When we assume that all the canonical states are eigenstates of the time-independent single-particle Hamiltonian  $h_0$ ,

$$|\phi_k(t)\rangle = |\phi_k^0\rangle e^{i\theta_k(t)}, \quad |\phi_{\bar{k}}(t)\rangle = |\phi_{\bar{k}}^0\rangle e^{i\theta_{\bar{k}}(t)}, \quad (37)$$

$$h_0 |\phi_k^0\rangle = \epsilon_k^0 |\phi_k^0\rangle, \quad h_0 |\phi_{\bar{k}}^0\rangle = \epsilon_{\bar{k}}^0 |\phi_{\bar{k}}^0\rangle, \quad (38)$$

where  $|\phi_{\bar{k}}\rangle = T|\phi_k\rangle$  have the same eigenvalues  $\epsilon_k^0$  as  $|\phi_k\rangle$ . Here,  $d\theta_k/dt = i \langle \partial \phi_k / \partial t | \phi_k \rangle$  and  $d\theta_{\bar{k}}/dt = i \langle \partial \phi_{\bar{k}} / \partial t | \phi_{\bar{k}} \rangle$  are arbitrary real functions of  $t$ .  $\kappa_k(t)$  and  $\Delta_k(t)$  should have a common time-dependent phase associated with the chemical potential  $\lambda$  as  $e^{-2i\lambda t}$ . In addition to this, according to their definitions, Eqs. (21) and (24) have the following additional phases connected with the phases of the canonical states:

$$\kappa_k(t) = \kappa_k^0 \exp\{-i[2\lambda t + \theta_k(t) + \theta_{\bar{k}}(t)]\}, \quad (39)$$

$$\Delta_k(t) = \Delta_k^0 \exp\{-i[2\lambda t + \theta_k(t) + \theta_{\bar{k}}(t)]\}, \quad (40)$$

The stationary case of Eq. (23)  $d\rho_k^0/dt = 0$  indicates that  $\kappa_k^0$  and  $\Delta_k^0$  have the same arguments to make  $\kappa_k(t)\Delta_k^*(t)$  real. If all the pairing matrix elements are real, we can choose that both  $\kappa_k^0$  and  $\Delta_k^0$  are real. Then, Eq. (27) reduces to

$$2(\epsilon_k^0 - \lambda)\kappa_k^0 + \Delta_k^0(2\rho_k^0 - 1) = 0. \quad (41)$$

This is consistent with the ordinary BCS result:

$$\rho_k^0 = \frac{1}{2} \left[ 1 - \frac{\epsilon_k^0 - \lambda}{\sqrt{(\epsilon_k^0 - \lambda)^2 + (\Delta_k^0)^2}} \right], \quad (42)$$

$$\kappa_k^0 = \frac{1}{2} \frac{\Delta_k^0}{\sqrt{(\epsilon_k^0 - \lambda)^2 + (\Delta_k^0)^2}}. \quad (43)$$

## D. Small-amplitude limit and the Nambu-Goldstone modes

It is known that the small-amplitude approximation for the TDHFB around the Hartree-Fock-Bogoliubov (HFB) ground state is identical to the QRPA. In the QRPA, when the ground state (HFB state) breaks continuous symmetry of the Hamiltonian, the Nambu-Goldstone modes appear as the zero-energy modes. In this section, we show that this is also true for the small-amplitude limit of the Cb-TDHFB.

The ground state is given by  $|\phi_k^0\rangle$ ,  $|\phi_{\bar{k}}^0\rangle$ ,  $\kappa_k^0$ , and  $\rho_k^0$ , which satisfy Eqs. (38) and (41). By extracting trivial phase factors  $\xi_k(t) \equiv \int_0^t \{\eta_k(t') - \epsilon_k^0\} dt'$ , we express the time-dependent quantities as follows:

$$|\phi_k(t)\rangle = \{ |\phi_k^0\rangle + |\delta\phi_k(t)\rangle \} e^{i\xi_k(t)}, \quad (44)$$

$$|\phi_{\bar{k}}(t)\rangle = \{ |\phi_{\bar{k}}^0\rangle + |\delta\phi_{\bar{k}}(t)\rangle \} e^{i\xi_{\bar{k}}(t)},$$

$$\kappa_k(t) = \{ \kappa_k^0 + \delta\kappa_k(t) \} e^{-i\{\xi_k(t) + \xi_{\bar{k}}(t) + 2\lambda t\}}, \quad (45)$$

$$\Delta_k(t) = \{ \Delta_k^0 + \delta\Delta_k(t) \} e^{-i\{\xi_k(t) + \xi_{\bar{k}}(t) + 2\lambda t\}},$$

$$\rho_k(t) = \rho_k^0 + \delta\rho_k(t), \quad h(t) = h_0 + \delta h(t), \quad (46)$$

By substituting these into Eqs. (23), (29), and (27), they lead to the following equations in the linear order with respect to

the fluctuation:

$$i \frac{\partial}{\partial t} |\delta\phi_k(t)\rangle = (h_0 - \epsilon_k^0) |\delta\phi_k(t)\rangle + \delta h(t) |\phi_k^0\rangle, \quad (k \leftrightarrow \bar{k}), \quad (47)$$

$$i \frac{\partial}{\partial t} \delta\rho_k(t) = \Delta_k^{0*} \delta\kappa_k(t) + \kappa_k^0 \delta\Delta_k^*(t) - \text{c.c.}, \quad (48)$$

$$i \frac{\partial}{\partial t} \delta\kappa_k(t) = 2(\epsilon_k^0 - \lambda) \delta\kappa_k(t) + (2\rho_k^0 - 1) \delta\Delta_k(t) + 2\Delta_k^0 \delta\rho_k(t). \quad (49)$$

When these fluctuating parts have specific oscillating frequency  $\omega$ , they correspond to the normal modes. The zero-energy modes correspond to stationary normal-mode solutions with  $\omega = 0$ .

### 1. Translation and rotation

When the HFB ground state spontaneously violates the translational (rotational) symmetry, there are generators  $\vec{P}$  ( $\vec{J}$ ), which transform the ground state into a new state but keep the energy invariant. Here, let us denote one of those Hermitian generators  $S$ . The transformation with respect to the generator  $S$  with real parameter  $\alpha$  leads to

$$|\phi_k^0\rangle \rightarrow |\phi_k^0(\alpha)\rangle = e^{i\alpha S} |\phi_k^0\rangle \quad (k \leftrightarrow \bar{k}), \quad (50)$$

$$h_0 \rightarrow h_0(\alpha) = e^{i\alpha S} h_0 e^{-i\alpha S}, \quad (51)$$

with  $\rho_k(\alpha) = \rho_k^0$ ,  $\kappa_k(\alpha) = \kappa_k^0$ ,  $\epsilon_k(\alpha) = \epsilon_k^0$ , and  $\Delta_k(\alpha) = \Delta_k^0$ . These transformed quantities should also satisfy Eq. (38):

$$[h_0(\alpha) - \epsilon_k^0] |\phi_k^0(\alpha)\rangle = 0. \quad (52)$$

In the linear order with respect to the parameter  $\alpha$ , we have

$$i\alpha(h_0 - \epsilon_k^0)S |\phi_k^0\rangle + i\alpha[S, h_0] |\phi_k^0\rangle = 0. \quad (53)$$

Equation (53) means that  $|\delta\phi_k^S\rangle \equiv i\alpha S |\phi_k^0\rangle$  and  $\delta h_S \equiv i\alpha[S, h_0]$  correspond to a normal-mode solution with  $\omega = 0$  for Eq. (47).  $\delta\rho_k^S = 0$ ,  $\delta\kappa_k^S = 0$ , and  $\delta\Delta_k^S = 0$  also satisfy Eqs. (48) and (49). Therefore, the Nambu-Goldstone modes related to the spontaneous breaking of the translational and rotational symmetries become zero-energy modes in the small-amplitude Cb-TDHFB equations.

### 2. Pairing rotation

When the ground state is in the superfluid phase, we have  $\kappa_k^0 \neq 0$  at least for a certain  $k$ . The ground state can be transformed into a new state by the operation of  $e^{i\theta N}$  where  $N$  is the number operator. This transformation changes the phase of  $\kappa_k$  and  $\Delta_k$  but keeps the other quantities invariant:

$$\delta\kappa_k^N = e^{2i\theta} \kappa_k^0 - \kappa_k^0 \approx 2i\theta \kappa_k^0, \quad (54)$$

$$\delta\Delta_k^N = e^{2i\theta} \Delta_k^0 - \Delta_k^0 \approx 2i\theta \Delta_k^0,$$

$$\delta\rho_k^N = \delta h_N = 0, \quad |\delta\phi_k^N\rangle = |\delta\phi_k^N\rangle = 0. \quad (55)$$

By using Eq. (41), it is easy to see that these quantities correspond to an  $\omega = 0$  solution of Eqs. (47), (48), and (49). Thus, the pairing rotational modes appear as the zero-energy modes as well.

### 3. P-p (h-h) RPA

The Cb-TDHFB equation Eq. (47) seems to be independent of the rest of Eqs. (48) and (49), at first sight. However, this is not true, in general, because  $\delta\Delta_k(t)$  depends on  $|\delta\phi_k(t)\rangle$  and  $\delta h(t)$  depends on  $\delta\rho_k(t)$ . In contrast, when the ground state is in the normal phase ( $\kappa_k^0 = \Delta_k^0 = 0$ ),  $\delta\Delta_k(t)$  becomes independent of  $|\delta\phi_l(t)\rangle$ , and we have  $\delta\rho_k(t) = 0$ . This means that the particle-hole (p-h) channel is exactly decoupled from the p-p and h-h channels. It is well known that TDHF equations in the small-amplitude limit Eq. (47) reduce to the RPA equation in the p-h channel [8,15,16]. Thus, here, we discuss properties of the p-p and h-h channels.

The p-p and h-h dynamics are described by the following equations:

$$i \frac{\partial}{\partial t} \delta\kappa_k(t) = 2\epsilon_k^0 \delta\kappa_k(t) \pm \delta\Delta_k(t), \quad (56)$$

where the sign  $+$  ( $-$ ) is for hole (particle) orbitals, and we omit the chemical potential  $\lambda$ . For the p-p channel ( $\omega = E_{N+2} - E_N$ ), a normal mode with frequency  $\omega$  is described by  $\delta\kappa_p = X_p e^{-i\omega t}$  for particle orbitals ( $|p| > N/2$ ) and by  $\delta\kappa_h = -Y_h e^{-i\omega t}$  for hole orbitals ( $|h| \leq N/2$ ). For the h-h channel ( $\omega = E_{N-2} - E_N$ ), it is described by  $\delta\kappa_h = X_h e^{-i\omega t}$  for hole orbitals ( $|h| \leq N/2$ ) and by  $\delta\kappa_p = -Y_p e^{-i\omega t}$  for particle orbitals ( $|k| > N/2$ ). Equation (56) can be rewritten in a matrix form as

$$\begin{pmatrix} 2\epsilon_p^0 \delta_{pp'} + \bar{v}_{p\bar{p}p'\bar{p}'} & -\bar{v}_{p\bar{p}h'\bar{h}'} \\ -\bar{v}_{h\bar{h}p'\bar{p}'} & -2\epsilon_h^0 \delta_{hh'} + \bar{v}_{h\bar{h}h'\bar{h}'} \end{pmatrix} \begin{pmatrix} Z_{p'} \\ Z_{h'} \end{pmatrix} = \omega \begin{pmatrix} 1 & 0 \\ 0 & -1 \end{pmatrix} \begin{pmatrix} Z_p \\ Z_h \end{pmatrix}, \quad (57)$$

where  $Z_p = X_p$  ( $Z_p = Y_p$ ) and  $Z_h = Y_h$  ( $Z_h = X_h$ ) for the p-p (h-h) channel. This is equivalent to the p-p and h-h RPA in the BCS approximation [15].

## IV. Cb-TDHFB EQUATIONS WITH A SIMPLE PAIRING ENERGY FUNCTIONAL AND GAUGE CONDITION

### A. Pairing energy functional

Normally, the pairing energy functional is bilinear with respect to  $\kappa_{\mu\nu}$  and  $\kappa_{\mu\nu}^*$ . For instance, when it is calculated from the two-body interaction, it is given by

$$E_\kappa(t) = \sum_{\mu,\nu,\rho,\sigma} v_{\mu\nu,\rho\sigma} \kappa_{\mu\nu}^*(t) \kappa_{\rho\sigma}(t). \quad (58)$$

Thus, the pairing energy can also be written as

$$E_\kappa(t) = \frac{1}{2} \sum_{\mu\nu} \kappa_{\mu\nu}(t) \Delta_{\mu\nu}^*(t) = \frac{1}{2} \sum_{\mu\nu} \kappa_{\mu\nu}^*(t) \Delta_{\mu\nu}(t) \quad (59)$$

$$= - \sum_{k>0} \kappa_k(t) \Delta_k^*(t) = - \sum_{k>0} \kappa_k^*(t) \Delta_k(t). \quad (60)$$

For numerical calculations in the present paper, we adopt a schematic pairing functional in the form of

$$E_g(t) = - \sum_{k,l>0} G_{kl} \kappa_k^*(t) \kappa_l(t) = - \sum_{k>0} \kappa_k^*(t) \Delta_k(t), \quad (61)$$

$$\Delta_k(t) = \sum_{l>0} G_{kl} \kappa_l(t),$$

where  $G_{kl}$  is a Hermitian matrix. This pairing functional produces a pair potential that is diagonal in the Cb. This is consistent with the approximation of Eq. (28). However, the functional violates the gauge invariance Eq. (31) because

$$\sum_{l>0} G_{kl} e^{-i\theta_l + \theta_l} \kappa_l(t) \neq e^{-i\theta_k + \theta_k} \sum_{k>0} G_{kl} \kappa_l(t). \quad (62)$$

The violation comes from the fact that the  $\Delta_k(t)$  in this schematic definition no longer hold the correct phase relation to canonical states  $(k, \bar{k})$ , according to the definition of Eq. (24). Therefore, we require the gauge condition of  $\langle \frac{\partial \phi_k}{\partial t} | \phi_k \rangle = \langle \frac{\partial \phi_{\bar{k}}}{\partial t} | \phi_{\bar{k}} \rangle = 0$  to minimize the phase change of canonical states. This means that we choose the gauge parameters  $\eta_k(t)$  as

$$\begin{aligned} \eta_k(t) &= \epsilon_k(t) = \langle \phi_k(t) | h(t) | \phi_k(t) \rangle, \\ \eta_{\bar{k}}(t) &= \epsilon_{\bar{k}}(t) = \langle \phi_{\bar{k}}(t) | h(t) | \phi_{\bar{k}}(t) \rangle. \end{aligned} \quad (63)$$

### B. Properties of Cb-TDHFB equations with $E_g$

The Cb-TDHFB equations with the simple pairing functional Eq. (61) keep the following desired properties, if we adopt the special gauge condition Eq. (63). The details are presented in the Appendix.

- (i) Conservation law
  - (a) Conservation of orthonormal property of the canonical states
  - (b) Conservation of average particle number
  - (c) Conservation of average total energy
- (ii) The stationary solution corresponds to the HF+BCS solution.
- (iii) Small-amplitude limit
  - (a) The Nambu-Goldstone modes are zero-energy normal-mode solutions.
  - (b) If the ground state is in the normal phase, the equations are identical to the p-h, p-p, and h-h RPA with the BCS approximation.

Among these properties, i(a) and i(b) do not depend on the choice of the gauge, however, the other properties are guaranteed only with the special choice of gauge Eq. (63).

## V. DETAILS OF NUMERICAL CALCULATIONS

### A. Treatment of the pairing energy functional

In numerical calculations, we start from the HF+BCS calculation for the ground state. The pairing energy is calculated for the constant monopole pairing interaction with a smooth truncation for the model space. We follow the prescription given by Tajima *et al.* [17], which is equivalent to the following choice of  $G_{kl}$  from Eq. (61),

$$G_{kl} = gf(\epsilon_k^0) f(\epsilon_l^0), \quad (64)$$

with a constant real parameter  $g$ . The cutoff function  $f(\epsilon)$ , which depends on the ground-state single-particle energies, is

in the following form:

$$f(\epsilon) = \left[ 1 + \exp\left(\frac{\epsilon - \epsilon_c}{0.5 \text{ MeV}}\right) \right]^{-1/2} \theta(\epsilon_c - \epsilon), \quad (65)$$

with the cutoff energies,

$$\epsilon_c = \tilde{\lambda} + 5.0 \text{ MeV}, \quad e_c = \epsilon_c + 2.3 \text{ MeV}, \quad (66)$$

where  $\tilde{\lambda}$  is the average of the highest occupied level and the lowest unoccupied level in the HF state. Here, the cutoff parameter  $e_c$  is necessary to prevent occupation of spatially unlocalized single-particle states, known as the problem of unphysical gas near the drip line. For neutrons, if  $e_c$  becomes positive, we replace it by zero.

To determine the pairing strength constant  $g$  for each nuclei, we again follow the prescription of Ref. [17], which is practically identical to the one in Ref. [18]. For light nuclei ( $A < 50$ ), we replace  $g$  with 0.6 MeV when the calculated value exceeds 0.6 MeV. The pairing force strengths  $G_{kl}$  are calculated for the ground state and are kept constant during the time evolution. We define the state-independent pairing gap as follows:

$$\Delta(t) \equiv g \sum_{k>0} \kappa_k(t) f(\epsilon_k^0). \quad (67)$$

The gap parameter for each canonical pair of states  $k$  and  $\bar{k}$  can be written as  $\Delta_k(t) = \Delta(t) f(\epsilon_k^0)$ .

### B. Energy density functional and coordinate-space representation

In the present calculations, we adopt a Skyrme energy functional  $E_{\text{Sky}}[\rho]$  with the parameter set of SkM\* [19]. The functional contains both time-even and time-odd densities, the same as Ref. [20]. The pairing energy functional is added to this to give the total energy functional  $E[\rho, \kappa] = E_{\text{Sky}}[\rho] + E_g[\kappa]$ .

We use the Cartesian coordinate-space representation for the canonical states  $\phi_k(\vec{r}, \sigma; t) = \langle \vec{r}, \sigma | \phi_k(t) \rangle$  with  $\sigma = \pm 1/2$ . The three-dimensional (3D) coordinate space is discretized in a square mesh of  $\Delta x = \Delta y = \Delta z = 0.8$  fm in a sphere with a radius of 12 fm. Thus, each canonical state is represented by  $\phi_k(i, j, k, \sigma; t)$  with three discrete indexes for the 3D space.

### C. Calculation for the ground state

First, we need to obtain a static solution to construct an initial state for the time-dependent calculation. The numerical procedure is as follows:

- (i) Solve Eq. (38) for occupied canonical states ( $|k| \leq N/2$ ) with  $\rho_k = 1$ , and construct the HF Hamiltonian  $h_0[\rho]$  by using the imaginary-time method [21].
- (ii) Calculate unoccupied canonical states  $\phi_k^0(\vec{r}, \sigma)$  ( $|k| > N/2$ ) below the energy cutoff  $e_c$  by using the imaginary-time method with  $h_0$ .
- (iii) Solve the BCS equations [15] to obtain  $\rho_k$  and  $\kappa_k$ .
- (iv) Update  $h_0[\rho]$  with new  $\rho_k$ , then solve Eq. (38) again with the imaginary-time method to calculate canonical states with  $\epsilon_k^0 < e_c$ .
- (v) Back to 3. and repeat until convergence.

To solve Eq. (38), the imaginary-time-evolution operator for a small time interval  $\Delta t$  is repeatedly operated on each single-particle wave function. After each evolution, the single-particle wave functions are orthonormalized with the Gram-Schmidt method from low- to high-energy states. We add the constraints for the center of mass  $\int \vec{r} \rho(\vec{r}) = 0$  and the principal axis  $\int r_i r_j \rho(\vec{r}) = 0$  ( $i \neq j$ ) for deformed nuclei.

#### D. Real-time calculation for strength functions

The canonical states in the ground state define the initial state for time evolution. To study the linear response, we use a weak instantaneous external field of  $V_{\text{ext}}(\vec{r}, t) = -\eta F(\vec{r})\delta(t)$  to start the time evolution. Here,  $F(\vec{r})$  is a one-body field, such as an  $E1$  operator with recoil charges,

$$F_i(\vec{r}) = \begin{cases} (Ne/A)r_i & \text{for protons} \\ -(Ze/A)r_i & \text{for neutrons} \end{cases}, \quad (68)$$

where  $i = (x, y, z)$ . We also study the isoscalar quadrupole response with

$$F(\vec{r}) = \frac{1}{\sqrt{2(1 + \delta_{K0})}} \{r^2 Y_{2K}(\hat{\mathbf{r}}) + r^2 Y_{2-K}(\hat{\mathbf{r}})\}, \quad (69)$$

$K = 0$  and  $2$ .

Then, at time  $t = 0+$ , the canonical states are given by

$$\begin{aligned} \phi_k(\vec{r}, \sigma; t = 0+) &= e^{i\eta F(\vec{r})} \phi_k^0(\vec{r}, \sigma), \\ \phi_{\bar{k}}(\vec{r}, \sigma; t = 0+) &= e^{i\eta F(\vec{r})} \phi_{\bar{k}}^0(\vec{r}, \sigma), \end{aligned} \quad (70)$$

and the BCS factors are given by

$$\rho_k(t = 0+) = \rho_k^0, \quad \kappa_k(t = 0+) = \kappa_k^0. \quad (71)$$

The parameter  $\eta$  controls the strength of the external field. In this paper, since we calculate the linear response, it should be small enough to validate the linearity.

To solve the Cb-TDHFB equations in real time, we use the simple Euler algorithm:

$$i\phi_k(t + 2dt) = i\phi_k(t) + \{h(t + dt) - \epsilon_k(t + dt)\}\phi_k(t + dt) \times 2dt, \quad (72)$$

$$i\rho_k(t + 2dt) = i\rho_k(t) + \{\kappa_k(t + dt)\Delta_k^*(t + dt) - \text{c.c.}\} \times 2dt, \quad (73)$$

$$\begin{aligned} i\kappa_k(t + 2dt) &= i\kappa_k(t) + [\kappa_k(t + dt)\{\epsilon_k(t + dt) \\ &\quad + \epsilon_{\bar{k}}(t + dt) - 2\lambda\} + \Delta_k(t + dt) \\ &\quad \times \{2\rho_k(t + dt) - 1\}] \times 2dt. \end{aligned} \quad (74)$$

Here, we insert the chemical potential in Eq. (27), which cancels a global time-dependent phase at the ground state  $e^{-2i\lambda t}$  for  $\kappa_k$  and  $\Delta_k$ . To construct the states at the first step of  $t = dt$ , we use the fourth-order Taylor expansion of the time-evolution operator for the canonical states [2] and use the Euler method for  $\rho_k(dt)$  and  $\kappa_k(dt)$ . The time step  $dt$  is  $0.0005 \text{ MeV}^{-1}$ . The time evolution is calculated up to  $T = 10 \text{ MeV}^{-1}$ .

The strength function with respect to the operator  $F$  is calculated with the following formula [2]:

$$\begin{aligned} S(E; F) &\equiv \sum_n |\langle \Phi_n | F | \Phi_0 \rangle|^2 \delta(E - \tilde{E}_n) = -\frac{1}{\pi\eta} \text{Im} f(E), \\ \tilde{E}_n &> 0, \end{aligned} \quad (75)$$

where  $\tilde{E}_n = E_n - E_0$  and  $f(E)$  is defined by

$$f(E) = \int_0^\infty dt e^{i(E - \Gamma/2)t} \int F(\vec{r}) \{\rho(\vec{r}, t) - \rho(\vec{r}, 0)\} d\vec{r}, \quad (76)$$

where we have introduced a smoothing parameter  $\Gamma$ , which is set to  $1 \text{ MeV}$  throughout the calculations in Sec. VI. The formula can be obtained from the time-dependent perturbation theory in the first order with respect to  $\eta$  [2]. Note that the strength function  $S(E; F)$  is independent of the magnitude of the parameter  $\eta$  as far as the linear approximation is valid. In the present paper, we adopt the value of  $\eta = 10^{-4} \text{ fm}^{-1}$  for the  $E1$  operator and  $\eta = 10^{-3} \text{ fm}^{-2}$  for the quadrupole operator.

## VI. NUMERICAL RESULTS OF LINEAR-RESPONSE CALCULATION

In this paper, we apply the Cb-TDHFB method to the calculation of the strength functions for Ne and Mg isotopes. First, in Table I, we show calculated ground-state properties; deformations, chemical potentials, and gap energies defined by Eq. (67). These nuclei show a variety of shapes (spherical, prolate, oblate, and triaxial), with and without superfluidity. For nuclei in the superfluid phase with  $\Delta \neq 0$ , the numbers of canonical orbitals  $M_\tau$  included in the calculation ( $e_k^0 < e_c$ ) are as follows: For protons,  $M_p = 16$  for  $^{24,26,28}\text{Ne}$  and for

TABLE I. Calculated ground-state properties of Ne and Mg isotopes; quadrupole deformation parameters ( $\beta, \gamma$ ), pairing gaps Eq. (67) for neutrons and protons ( $\Delta_n, \Delta_p$ ), and chemical potentials for neutrons and protons ( $\lambda_n, \lambda_p$ ). In the case of normal phase ( $\Delta = 0$ ), we define the chemical potential as the single-particle energy of the highest occupied orbital  $\lambda_n = \epsilon_n^0$  and  $\lambda_p = \epsilon_p^0$ . The pairing gaps and chemical potentials are given in units of megaelectron volts.

	$\beta$	$\gamma$	$\Delta_n$	$\Delta_p$	$-\lambda_n$	$-\lambda_p$
$^{20}\text{Ne}$	0.37	$0^\circ$	0.0	0.0	13.07	9.19
$^{22}\text{Ne}$	0.37	$0^\circ$	0.0	0.0	11.03	12.38
$^{24}\text{Ne}$	0.17	$60^\circ$	0.0	0.74	10.57	13.04
$^{26}\text{Ne}$	0.0	–	0.0	1.00	7.17	14.92
$^{28}\text{Ne}$	0.0	–	0.79	1.01	3.22	17.05
$^{30}\text{Ne}$	0.0	–	1.37	1.01	2.41	19.09
$^{32}\text{Ne}$	0.36	$0^\circ$	0.95	0.0	2.16	23.61
$^{24}\text{Mg}$	0.39	$0^\circ$	0.0	0.0	14.12	9.51
$^{26}\text{Mg}$	0.20	$54^\circ$	0.0	0.86	13.08	11.23
$^{28}\text{Mg}$	0.0	–	0.0	1.03	9.21	13.30
$^{30}\text{Mg}$	0.0	–	1.31	1.03	5.48	15.49
$^{32}\text{Mg}$	0.01	–	1.62	1.03	4.52	17.50
$^{34}\text{Mg}$	0.37	$0^\circ$	1.45	0.0	4.12	20.18
$^{36}\text{Mg}$	0.33	$0^\circ$	1.43	0.0	3.21	21.95
$^{38}\text{Mg}$	0.30	$0^\circ$	1.47	0.0	2.38	23.69
$^{40}\text{Mg}$	0.29	$0^\circ$	0.91	0.0	1.31	25.28

$^{26,28,30,32}\text{Mg}$ , and  $M_p = 20$  for  $^{30}\text{Ne}$ . For neutrons,  $M_n = 20$  orbitals for  $^{28}\text{Ne}$ ,  $M_n = 24$  for  $^{32}\text{Ne}$ ,  $M_n = 28$  for  $^{30}\text{Ne}$  and for  $^{30,34,36}\text{Mg}$ , and  $M_n = 30$  for  $^{32,38,40}\text{Mg}$ . These numbers are, of course, larger than the proton and neutron numbers but not significantly different. In the case with  $\Delta = 0$ , of course, we only calculate the occupied orbitals ( $M_p = Z$  and  $M_n = N$ ). Therefore, the numerical task of the Cb-TDHFB is on the same order as that of the TDHF. Note that, in the real-time calculation, the numerical cost is proportional to  $M_n + M_p$ .

### A. Isoscalar quadrupole excitations: Comparison with QRPA calculations

We expect that the strength functions calculated in the present real-time approaches reproduce those in the QRPA. This is strictly true if we solve the full TDHFB equations, however, since we solve the Cb-TDHFB equations with the schematic pairing functional of Eq. (61) with Eq. (64), let us first show the comparison between our result and the HFB + QRPA calculations. The QRPA calculations have been performed with a computer program for axially deformed nuclei developed in Ref. [22], which diagonalizes the QRPA matrix of large dimensions in the quasiparticle basis. This is based on the HFB ground state calculated in the two-dimensional coordinate-space representation with the Skyrme functional SkM\* but with the density-dependent contact interaction for the pairing channel. The space is truncated by the quasiparticle energy cutoff of  $E_{\text{cut}} = 60$  MeV and also by the cutoff for the magnetic quantum number of the quasiparticle angular momentum  $\Omega_c = 19/2$ . In this QRPA calculation, the residual spin-orbit and Coulomb interactions are neglected. Thus, to make a comparison more meaningful, we also neglect the time dependence of these potentials in the Hamiltonian  $h(t)$  during the time evolution.

In panels (a) and (c) of Fig. 1, we show the isoscalar quadrupole strength distributions ( $K = 0$  and 2) for  $^{34}\text{Mg}$ ,

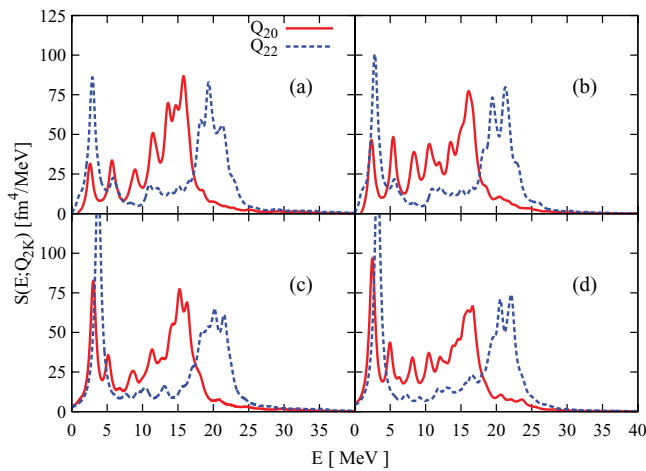


FIG. 1. (Color online) Calculated isoscalar quadrupole strength distribution for  $^{34}\text{Mg}$ : (a) Cb-TDHFB with time-independent spin-orbit and Coulomb potentials, (b) Cb-TDHFB, (c) deformed QRPA without the residual spin-orbit and Coulomb interactions [22], and (d) deformed QRPA calculation [23]. The smoothing parameter of  $\Gamma = 1$  MeV is used.

calculated with (a) Cb-TDHFB and (c) QRPA. The ground state has an axially symmetric prolate shape with finite pairing gaps for neutrons (Table I). The HFB calculation with the contact pairing interaction for the panel (c) produces a deformation and an average neutron pairing gap of  $\beta = 0.37$  and  $\Delta_n = 1.7$  MeV, respectively. Note that a renormalization factor, which was used in Ref. [22], is set to be unity in the present QRPA calculation. The peak energies in these calculations are approximately identical, however, the height of the lowest peak is noticeably different. We suppose that this is caused by the difference in the pairing energy functionals.

In panels (b) and (d) of Fig. 1, we show another comparison between the Cb-TDHFB calculation and the QRPA calculation of Losa *et al.* [23] by using the transformed harmonic oscillator basis. Since this QRPA calculation includes all the residual interactions, it is compared with the Cb-TDHFB calculation with the fully self-consistent time dependence. It turns out that the residual spin-orbit and Coulomb interactions slightly shift the giant quadrupole resonance higher in energy, while they shift the lowest peak lower in energy. Actually, these shifts are mainly attributed to the residual spin-orbit interaction, and the effect of the residual Coulomb is very small. The results in panels (b) and (d) well agree with each other, except for the height of the lowest peak. Again, this may be caused by the different treatment of the pairing because Ref. [23] also uses the contact pairing interaction. These comparisons indicate that the small-amplitude Cb-TDHFB calculation well reproduces a fully self-consistent QRPA calculation. We would like to mention that, for the isovector dipole excitations, the agreement is even better than for the isoscalar quadrupole cases.

### B. Isovector ( $E1$ ) dipole excitations

Here, we discuss properties of the isovector dipole excitations, which include low-energy pygmy dipole resonances and high-energy giant dipole resonances (GDRs). First, in Fig. 2,

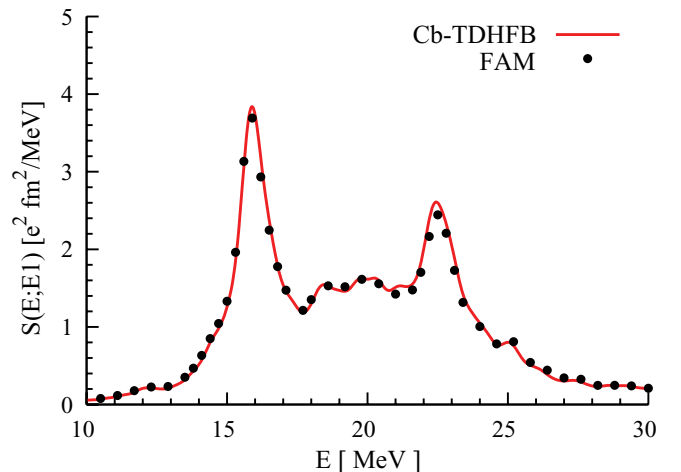


FIG. 2. (Color online)  $E1$  strength distribution for  $^{24}\text{Mg}$  calculated with the Cb-TDHFB (solid line) and with the FAM [16,24] (symbols). The smoothing parameter of  $\Gamma = 1$  MeV is used.

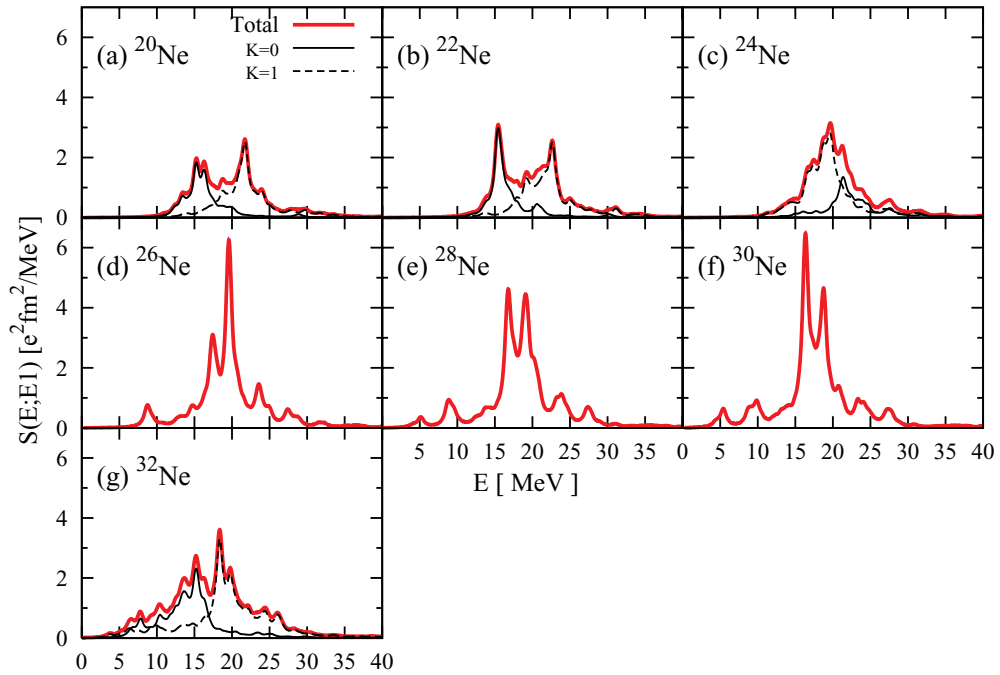


FIG. 3. (Color online) Calculated  $E1$  strength distribution for Ne isotopes. For deformed nuclei, the total strength Eq. (77) is decomposed into  $S_z[E; (E1)]$  (thin solid line) and  $S_x[E; (E1)] + S_y[E; (E1)]$  (dashed line). The  $z$  axis is the symmetry axis for axially deformed cases. The smoothing parameter of  $\Gamma = 1$  MeV is used.

let us show the comparison between results of the present Cb-TDHFB calculation and those of the RPA calculation. The fully self-consistent RPA calculation has been performed with the finite-amplitude method (FAM) developed in Refs. [16,24]. The same Skyrme functional (SkM\*) and the same model space have been used in these calculations. Since the ground

state of the  $^{24}\text{Mg}$  nucleus is in the normal phase ( $\Delta = 0$ ), these two results should be identical. This can be confirmed in Fig. 2, which clearly demonstrates the accuracy of our real-time method.

Next, in Fig. 3, we show the calculated  $E1$  strength distribution for Ne isotopes. Here,  $S(E; E1)$  is defined

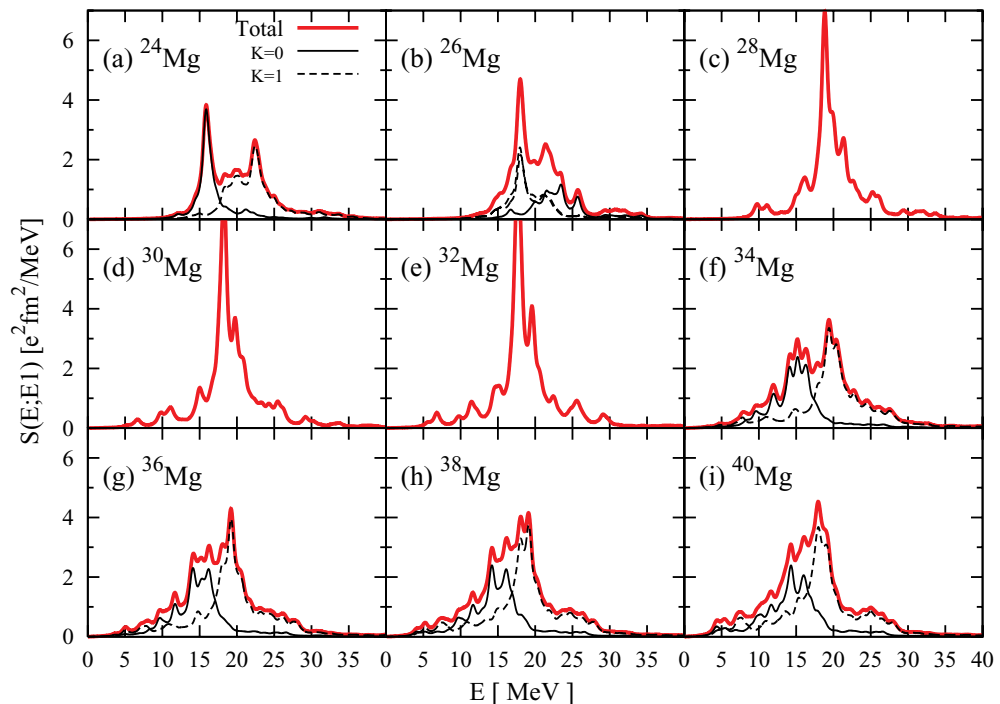


FIG. 4. (Color online) Same as Fig. 3 but for Mg isotopes.

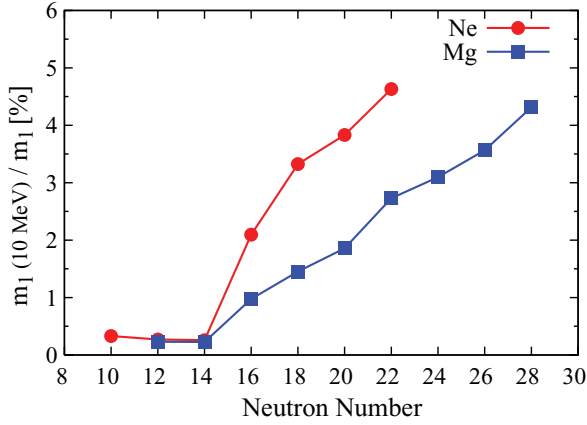


FIG. 5. (Color online) Ratio of low-energy  $E1$  energy-weighted sum value to the total sum value, as a function of neutron number. See text for details.

as

$$\begin{aligned}
 S(E; E1) &= \sum_{i=x,y,z} S_i(E; E1) \\
 &= \sum_{i=x,y,z} \sum_n |\langle n | F_i | 0 \rangle|^2 \delta(E - \tilde{E}_n), \quad (77)
 \end{aligned}$$

where the one-body operator  $F_i$  is given by Eq. (68). The  $K = 0$  strength is  $S_z(E; E1)$ , and  $K = 1$  corresponds to  $S_x(E; E1) + S_y(E; E1)$ . Here, for axially symmetric nuclei, the symmetry axis is chosen as the  $z$  axis. The ground states of  $^{20,22}\text{Ne}$  are deformed in a prolate shape with  $\Delta = 0$  for both protons and neutrons. Thus, the calculation is identical to the small-amplitude TDHF. Both nuclei show a prominent double-peak structure. The lower peak is located around 16 MeV, and the higher one is located around 22 MeV. This comes from the deformation splitting, and the lower peak is characterized as  $K = 0$ , and the higher one is characterized as  $K = 1$ . The similar structure is seen in the neutron-rich nucleus  $^{32}\text{Ne}$ . However, despite the fact that the magnitude of deformation is roughly the same as that of  $^{20,22}\text{Ne}$ , the position of the higher peak ( $K = 1$ ) is lowered, and the splitting is not as prominent as that in  $^{20,22}\text{Ne}$ . In oblate nuclei, such as  $^{24}\text{Ne}$ , the deformation splitting is not clearly seen in the total strength

distribution  $S(E; E1)$  because the high-energy peak becomes much smaller than the lower peak.

For  $^{24-32}\text{Ne}$ , calculated ground states are in the superfluid phase for either neutrons, protons, or both. Peak energies of the GDR gradually decrease as the neutron number increases, from about 20 to 17 MeV. We have confirmed that the pairing correlation does not significantly affect the  $E1$  strength distribution. However, for some cases, the ground-state deformation is changed by the presence of the pairing. For instance, the  $^{26}\text{Ne}$  nucleus is deformed in the prolate shape if we neglect the pairing correlations. In contrast, the present BCS calculation produces the spherical ground state.

The low-energy  $E1$  strength, which is often called pygmy resonance, is of significant interest. In Ne isotopes, there are two effects to create the low-energy  $E1$  strength: One is a large deformation splitting, which brings the lower peak down to around 15 MeV. Another effect comes from the neutron excess. In  $^{26-32}\text{Ne}$ , the pygmy peaks appear below 10 MeV. For  $^{26}\text{Ne}$ , this low-energy peak structure has recently been measured at RIKEN [25]. The calculated pygmy position is around 8 to 9 MeV, which agrees with experimental data [25] and with the other QRPA calculations [22,26]. For nuclei with even more neutrons ( $A \geq 28$ ), a double-peak structure below 10 MeV appears.

In Fig. 4,  $E1$  strength distributions for Mg isotopes are displayed.  $^{26}\text{Mg}$  is nearly oblate but has a triaxial shape with  $\gamma = 54^\circ$ . The low-energy peak at 18 MeV is prominent in this nucleus. In  $^{28}\text{Mg}$  and heavier isotopes, there are pygmy states below 10 MeV. As in Ne isotopes, a double-peak structure for  $A \geq 30$  appears, although the heights of these pygmy peaks in Mg are lower than those in Ne isotopes.

To investigate how the low-energy pygmy strength changes as the neutron number increases, we define the low-energy  $E1$  ratio by  $m_1(E_c)/m_1$  with  $E_c = 10$  MeV, where

$$m_1(E) \equiv \int_0^E E' S(E'; E1) dE', \quad (78)$$

and  $m_1 \equiv m_1(\infty)$ . This ratio is shown for calculated even-even Ne and Mg isotopes in Fig. 5. Both isotopes with  $N = 10-14$  have very little  $E1$  strength below 10 MeV. Then, the ratio  $m_1(E_c)/m_1$  shows a rapid increase as a function of the neutron number. Especially, we can see abrupt jumps between

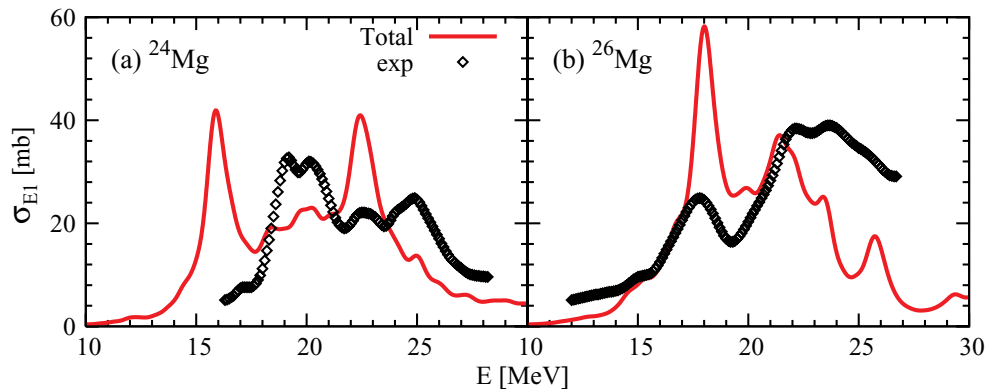


FIG. 6. (Color online) Photoabsorption cross sections for  $^{24,26}\text{Mg}$ . Experimental data (symbols) are taken from Ref. [27]. The smoothing parameter of  $\Gamma = 1$  MeV is used for the calculations.

$N = 14$  and  $16$  and between  $N = 20$  and  $22$ . The first jump between  $N = 14$  and  $16$  seems to be caused by occupation of the neutron  $s_{1/2}$  orbital. In contrast, the second jump between  $N = 20$  and  $22$  may be caused by the onset of the deformation and the neutron pairing. The low-energy strengths in Ne isotopes show roughly twice larger values compared with Mg nuclei with the same neutron numbers. This may be attributed to the difference in the separation energy (chemical potential).

Finally, let us present photoabsorption cross sections in the GDR energy region ( $E = 10$ – $30$  MeV) together with experimental data [27] (see Fig. 6). For  $^{24}\text{Mg}$ , the peak energies of the GDR are underestimated by about 3 MeV. This disagreement has already been found in Ref. [24] for  $^{24}\text{Mg}$ . The present calculation also indicates that this underestimation of the GDR peak energy is also true for  $^{26}\text{Mg}$ . The  $E1$  strength distribution for  $^{26}\text{Mg}$  is very similar to that in Fig. 12 (bottom panel) in Ref. [23]. In light nuclei, the GDR energy is systematically underestimated in most of the Skyrme functionals [24], which seems to be true for nuclei with superfluidity.

## VII. CONCLUSION

We have developed an approximate approach to the TDHFB theory by using the Cb representation for time evolution of the densities and pairing tensors. Although, in general, the pair potential is not in a diagonal form in the Cb, if it is approximated in such a form, the TDHFB equations can be enormously simplified, to give Cb-TDHFB equations. In this paper, we have treated a full Skyrme functional for the p-h channel; however, we have used a simple schematic functional for the pairing channel. Since the schematic pairing functional violates the gauge invariance, it requires a special choice for the gauge condition. The Cb-TDHFB equations contain the TDHF as a special case of the absence of pairing correlations. Its static limit is identical to the HF+BCS approximation. We have shown that the equations possess many of the desired properties analogous to the original TDHFB theory, which include conservation of the average particle number and the average total energy. We have also investigated analytical properties of its small-amplitude limit and found that the Nambu-Goldstone modes correspond to zero-energy normal modes and are automatically separated from other finite-energy modes.

We have developed a computational program for real-time propagation based on the Cb-TDHFB equations by using the 3D coordinate-space representation. To test the accuracy and validity of the present method, we have calculated the isoscalar quadrupole strength distribution in deformed  $^{34}\text{Mg}$  with the small-amplitude real-time method and compared it with deformed QRPA calculations by using a standard diagonalization method [22,23]. Results agree well with each other, except for the quadrupole strength of the lowest state located around 3 MeV. This may be caused by the difference of the pairing energy functional used in the Cb-TDHFB and QRPA calculations.

Then, we have calculated the  $E1$  strength distribution for even-even Ne and Mg isotopes systematically. The ground-state properties of these isotopes change from one nucleus to another. For instance, there are a variety of shapes, which include spherical, prolate, oblate, and triaxial deformations.

The gap energies also significantly change, which depend on the particle number and deformation. The 3D representation allows us to treat all of these nuclei in a self-consistent and systematic manner. Typical deformation splitting of the GDRs is predicted for prolate deformed nuclei  $^{20,22,32}\text{Ne}$  and  $^{24,34-40}\text{Mg}$ . The neutron-rich deformed nuclei, such as  $^{32}\text{Ne}$  and  $^{34-40}\text{Mg}$ , show a  $K = 0$  peak around 15 MeV and a significant strength in a low-energy tail at 5–10 MeV. The low-energy  $E1$  pygmy strength is almost negligible for  $^{20-24}\text{Ne}$  and  $^{24-26}\text{Mg}$  but suddenly starts to increase at the neutron number 16 with another jump at 22. This seems to be caused by the occupation of the neutron  $s_{1/2}$  orbital and the onset of the neutron pairing. The effect of the deformation also plays a role in the increase of the pygmy strength in the low-energy region. These low-energy  $E1$  strengths are of significant interest in studies of the element-synthesis reactions in stars and in explosive environments.

The Cb-TDHFB method is easily applicable to linear-response calculations for heavier systems. Its computational task is roughly the same as that of the TDHF. Furthermore, it will provide a useful tool to study heavy-ion collision dynamics beyond the TDHF, for instance, to investigate the dynamical pairing effects for dissipation. For this purpose, we need to make a few improvements over the present computer program: First, the simple pairing energy functional of Eq. (61) should be replaced by the one calculated from a more realistic interaction because this pairing functional induces unphysical coupling among nucleons spatially far apart. Next, we need to improve the code suitable for the massively parallel computing. The pairing rotation for colliding two different nuclei requires us to take an average over many initial states with different phases. Thus, even with the Cb-TDHFB method, the necessary computational resources will be significantly larger than the TDHF. These computational issues are rather straightforward to solve, and we suppose that they are tractable with the Cb-TDHFB method.

## ACKNOWLEDGMENTS

This work is supported by a Grant-in-Aid for Scientific Research(B) (Grant No. 21340073) and for innovative areas (Grant No. 20105003). Computational resources were provided by the PACS-CS project and the Joint Research Program (Projects No. 07b-7, No. 08a-8, No. 08b-24, No. 09b-9, No. 09a-25, and No. 10a-22) at the Center for Computational Sciences, University of Tsukuba, and by the Large Scale Simulation Program (Projects No. 07-20, No. 08-14, No. 09-16, and No. 09/10-10) of the High Energy Accelerator Research Organization (KEK). Computations were also performed on the RIKEN Integrated Cluster of Clusters (RICC). We acknowledge the JSPS Core-to-Core Program International Research Network for Exotic Femto Systems and the UNEDF SciDAC Collaboration under DOE Grant No. DE-FC02-07ER41457.

## APPENDIX: PROOF OF PROPERTIES OF Cb-TDHFB WITH $E_g$

Among the properties listed in Sec. IV B, the conservation of the orthonormal property and that of the particle number

are trivially identical to Sec. III. In the following, we show a simple proof of the other properties.

### 1. Average total energy conservation

By using the Cb-TDHFB equations, it is easy to show that the time derivative of the schematic pairing functional of Eq. (61) gives

$$\begin{aligned} i \frac{d}{dt} E_g &= -i \sum_{k,l>0} G_{kl} \left[ \frac{d\kappa_k^*}{dt} \kappa_l(t) + \kappa_k^*(t) \frac{d\kappa_l}{dt} \right] \\ &= -i \sum_{k>0} \frac{d\rho_k}{dt} [\eta_k(t) + \eta_{\bar{k}}(t)]. \end{aligned} \quad (\text{A1})$$

Only with the special choice of the gauge parameters Eq. (63), do we observe the conservation of the total energy.

### 2. Stationary solution

By following the arguments in Sec. III C, it is easy to see that the stationary solution corresponds to the ordinary HF+BCS result but only when we adopt the gauge fixing Eq. (63).

### 3. Small-amplitude limit

With the use of the pairing functional Eq. (61), we can no longer assume the time-dependent phase factor of Eq. (45) for  $\Delta_k(t)$ . Instead, we only extract the global phase related to the chemical potential from  $\kappa_k(t)$  and  $\Delta_k(t)$ :

$$\begin{aligned} |\phi_k(t)\rangle &= |\phi_k^0\rangle + |\delta\phi_k(t)\rangle, \quad |\phi_{\bar{k}}(t)\rangle = |\phi_{\bar{k}}^0\rangle + |\delta\phi_{\bar{k}}(t)\rangle, \quad (\text{A2}) \\ \kappa_k(t) &= \{\kappa_k^0 + \delta\kappa_k(t)\} e^{-2i\lambda t}, \\ \Delta_k(t) &= \{\Delta_k^0 + \delta\Delta_k(t)\} e^{-2i\lambda t}, \end{aligned} \quad (\text{A3})$$

$$\rho_k(t) = \rho_k^0 + \delta\rho_k(t), \quad h(t) = h_0 + \delta h(t). \quad (\text{A4})$$

By using the gauge condition Eq. (63), we have the following equations for the small-amplitude limit of the Cb-TDHFB equations:

$$i \frac{\partial}{\partial t} |\delta\phi_k(t)\rangle = (h_0 - \epsilon_k^0) |\delta\phi_k(t)\rangle + (1 - |\phi_k^0\rangle\langle\phi_k^0|) \delta h(t) |\phi_k^0\rangle, \quad (\text{A5})$$

$(k \leftrightarrow \bar{k}),$

$$i \frac{\partial}{\partial t} \delta\rho_k(t) = \Delta_k^0 \delta\kappa_k(t) + \kappa_k^0 \sum_{l>0} G_{kl} \delta\kappa_l(t) - \text{c.c.}, \quad (\text{A6})$$

$$\begin{aligned} i \frac{\partial}{\partial t} \delta\kappa_k(t) &= 2(\epsilon_k^0 - \lambda) \delta\kappa_k(t) + (|\phi_k^0\rangle\langle\phi_k^0| \delta h(t) |\phi_k^0\rangle \\ &\quad + \langle\phi_k^0| \delta h(t) |\phi_k^0\rangle) \kappa_k^0 + (2\rho_k^0 - 1) \sum_{l>0} G_{kl} \delta\kappa_l(t) \\ &\quad + 2\Delta_k^0 \delta\rho_k(t). \end{aligned} \quad (\text{A7})$$

Here, we used the equation  $\langle\phi_k^0 + \delta\phi_k(t)|[h_0 + \delta h(t)]|\phi_k^0 + \delta\phi_k(t)\rangle = \epsilon_k^0 + \langle\phi_k^0| \delta h(t) |\phi_k^0\rangle$ , which can be verified because of the norm conservation.

#### a. Translation and rotation

The same argument as that of Sec. III D1 leads to

$$i\alpha(h_0 - \epsilon_k^0) S |\phi_k^0\rangle + (1 - |\phi_k^0\rangle\langle\phi_k^0|) i\alpha[S, h_0] |\phi_k^0\rangle = 0, \quad (\text{A8})$$

where we multiply the projection  $(1 - |\phi_k^0\rangle\langle\phi_k^0|)$  on both sides of Eq. (53). Equation (A8) means that  $|\delta\phi_k^S\rangle \equiv i(1 - |\phi_k^0\rangle\langle\phi_k^0|) S |\phi_k^0\rangle$  and  $\delta h_S \equiv i[S, h_0]$  correspond to a zero-energy normal-mode solution for Eq. (A5). Note that  $|\delta\phi_k^S\rangle = i\alpha S |\phi_k^0\rangle$  and  $|\delta\phi_k^S\rangle$  produce the identical density fluctuation,  $\delta\rho_k = 0$  and  $\delta\kappa_k = 0$  also satisfy Eqs. (A6) and (A7), since  $\langle\phi_k^0| \delta h_S |\phi_k^0\rangle = i \langle\phi_k^0| [S, h_0] |\phi_k^0\rangle = 0$ . Therefore, the translational and rotational modes appear as the zero-energy normal modes.

#### b. Pairing rotation

When the ground state is in the superfluid phase, the transformation  $e^{i\theta N}$  changes the phase of  $\kappa_k$ :

$$\delta\kappa_k^N = e^{2i\theta} \kappa_k^0 - \kappa_k^0 \approx 2i\theta \kappa_k^0, \quad (\text{A9})$$

$$\delta\rho_k^N = \delta h_N = 0, \quad |\delta\phi_k^N\rangle = |\delta\phi_{\bar{k}}^N\rangle = 0. \quad (\text{A10})$$

By using Eq. (41), it is easy to see that these quantities correspond to a normal-mode solution with  $\omega = 0$  for Eqs. (A5)–(A7). Thus, the pairing rotational modes appear as the zero-energy modes. Again, without the gauge condition Eq. (63), we would not have this property.

#### c. P-p (h-h) RPA

In the case of  $\kappa_k^0 = 0$ , it is easy to see that the p-p (h-h) channels are decoupled from the p-h channels. The p-p and h-h dynamics are described by the following equation:

$$i \frac{\partial}{\partial t} \delta\kappa_k(t) = 2(\epsilon_k^0 - \lambda) \delta\kappa_k(t) \pm \sum_{l>0} G_{kl} \delta\kappa_l(t), \quad (\text{A11})$$

where the sign  $+$  ( $-$ ) is for hole (particle) orbitals. Again, by introducing the forward and backward amplitudes in the same manner as in Sec. III D3, Eq. (A11) can be rewritten in a matrix form as

$$\begin{pmatrix} 2\epsilon_p^0 \delta_{pp'} - G_{pp'} & G_{ph'} \\ G_{hp'} & -2\epsilon_h^0 \delta_{hh'} - G_{hh'} \end{pmatrix} \begin{pmatrix} Z_{p'} \\ Z_{h'} \end{pmatrix} = \omega \begin{pmatrix} 1 & 0 \\ 0 & -1 \end{pmatrix} \begin{pmatrix} Z_p \\ Z_h \end{pmatrix}, \quad (\text{A12})$$

where  $Z_p = X_p$  ( $Z_p = Y_p$ ) and  $Z_h = Y_h$  ( $Z_h = X_h$ ) for the p-p (h-h) channel.

- [1] J. W. Negele, *Rev. Mod. Phys.* **54**, 913 (1982).  
 [2] T. Nakatsukasa and K. Yabana, *Phys. Rev. C* **71**, 024301 (2005).  
 [3] J. A. Maruhn, P. G. Reinhard, P. D. Stevenson, J. R. Stone, and M. R. Strayer, *Phys. Rev. C* **71**, 064328 (2005).  
 [4] A. S. Umar and V. E. Oberacker, *Phys. Rev. C* **73**, 054607 (2006).

- [5] A. S. Umar and V. E. Oberacker, *Phys. Rev. C* **76**, 014614 (2007).  
 [6] K. Washiyama and D. Lacroix, *Phys. Rev. C* **78**, 024610 (2008).  
 [7] C. Golabek and C. Simenel, *Phys. Rev. Lett.* **103**, 042701 (2009).  
 [8] J.-P. Blaizot and G. Ripka, *Quantum Theory of Finite Systems* (MIT Press, Cambridge, MA, 1986).

- [9] Y. Hashimoto and K. Nodeki, [arXiv:0707.3083](#).
- [10] B. Avez, C. Simenel, and P. Chomaz, [Phys. Rev. C \*\*78\*\*, 044318 \(2008\)](#).
- [11] J. Błocki and H. Flocard, [Nucl. Phys. A \*\*273\*\*, 45 \(1976\)](#).
- [12] J. W. Negele, S. E. Koonin, P. Möller, J. R. Nix, and A. J. Sierk, [Phys. Rev. C \*\*17\*\*, 1098 \(1978\)](#).
- [13] R. Y. Cusson and H. W. Meldner, [Phys. Rev. Lett. \*\*42\*\*, 694 \(1979\)](#).
- [14] R. Y. Cusson, J. A. Maruhn, and H. W. Meldner, [Z. Phys. A \*\*294\*\*, 257 \(1980\)](#).
- [15] P. Ring and P. Schuck, *The Nuclear Many-Body Problems*, Texts and Monographs in Physics (Springer-Verlag, New York, 1980).
- [16] T. Nakatsukasa, T. Inakura, and K. Yabana, [Phys. Rev. C \*\*76\*\*, 024318 \(2007\)](#).
- [17] N. Tajima, S. Takahara, and N. Onishi, [Nucl. Phys. A \*\*603\*\*, 23 \(1996\)](#).
- [18] M. Brack, J. Damgaard, A. S. Jensen, H. C. Pauli, V. M. Strutinsky, and C. Y. Wong, [Rev. Mod. Phys. \*\*44\*\*, 320 \(1972\)](#).
- [19] J. Bartel, P. Quentin, M. Brack, C. Guet, and H. Håkansson, [Nucl. Phys. A \*\*386\*\*, 79 \(1982\)](#).
- [20] P. Bonche, H. Flocard, and P. H. Heenen, [Nucl. Phys. A \*\*467\*\*, 115 \(1987\)](#).
- [21] K. T. R. Davies, H. Flocard, S. Krieger, and M. S. Weiss, [Nucl. Phys. A \*\*342\*\*, 111 \(1980\)](#).
- [22] K. Yoshida and N. V. Giai, [Phys. Rev. C \*\*78\*\*, 064316 \(2008\)](#).
- [23] C. Losa, A. Pastore, T. Døssing, E. Vigezzi, and R. A. Broglia, [Phys. Rev. C \*\*81\*\*, 064307 \(2010\)](#).
- [24] T. Inakura, T. Nakatsukasa, and K. Yabana, [Phys. Rev. C \*\*80\*\*, 044301 \(2009\)](#).
- [25] J. Gibelin *et al.*, [Phys. Rev. Lett. \*\*101\*\*, 212503 \(2008\)](#).
- [26] L.-G. Cao and Z.-Y. Ma, [Phys. Rev. C \*\*71\*\*, 034305 \(2005\)](#).
- [27] V. V. Varlamov, M. E. Stepanov, and V. V. Chesnokov, [Bull. Rus. Acad. Sci. Phys. \*\*67\*\*, 724 \(2003\)](#).